Nanoscale

This is an *Accepted Manuscript*, which has been through the RSC Publishing peer review process and has been accepted for publication.

Accepted Manuscripts are published online shortly after acceptance, which is prior to technical editing, formatting and proof reading. This free service from RSC Publishing allows authors to make their results available to the community, in citable form, before publication of the edited article. This *Accepted Manuscript* will be replaced by the edited and formatted *Advance Article* as soon as this is available.

To cite this manuscript please use its permanent Digital Object Identifier (DOI®), which is identical for all formats of publication.

More information about *Accepted Manuscripts* can be found in the **Information for Authors**.

Please note that technical editing may introduce minor changes to the text and/or graphics contained in the manuscript submitted by the author(s) which may alter content, and that the standard **Terms & Conditions** and the **ethical guidelines** that apply to the journal are still applicable. In no event shall the RSC be held responsible for any errors or omissions in these *Accepted Manuscript* manuscripts or any consequences arising from the use of any information contained in them.
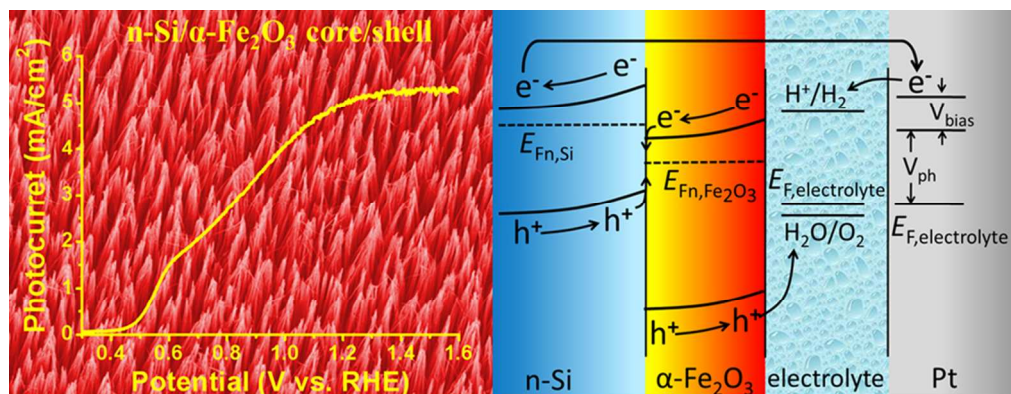
82x32mm (300 x 300 DPI)

Nanoscale

ARTICLE

High-Performance n-Si/α-Fe₂O₃ Core/Shell Nanowire Array Photoanode towards Photoelectrochemical Water Splitting

Xiaopeng Qi,[ab] Guangwei She,[*a] Xing Huang,[a] Taiping Zhang,[a] Huimin Wang,[a] Lixuan Mu[a] and Wensheng Shi[*a]

Many narrow band-gap semiconductors cannot fulfill the energetic requirements for water splitting, thus the assistance of large external voltages to complete the water decomposition reaction is required. Through thermal decomposition of $Fe(NO_3)_3$ on n-Si nanowires prepared by the chemical etching method, we fabricated a high-performance n-Si/α-Fe₂O₃ core/shell nanowire array photoanode that exhibited a low photocurrent onset potential of 0.5 V vs RHE and a high photocurrent of 5.28 mA/cm² at 1.23V vs RHE, under simulated AM 1.5G irradiation. The photocurrent onset potential represents one of the lowest in n-Si or α-Fe₂O₃ based photoanodes, and the photocurrent is much larger than most of those observed on α-Fe₂O₃. The impact of the thickness of the α-Fe₂O₃ shell on the photoelectrochemical performance of the present photoanode was investigated in detail. It was found that both the photocurrent and the onset potential depend strongly on the α-Fe₂O₃ shell thickness. Mott-Schottky measurements and energy band calculation reveal that the energy band edge positions of the n-Si are closely related to the thickness of the α-Fe₂O₃. The α-Fe₂O₃ shell with an optimized thickness is favorable for locating the energy bands of the n-Si at relatively high levels and maximizing the charge collection in α-Fe₂O₃, and thus achieving the low photocurrent onset potential and high photocurrent.

Introduction

Photoelectrochemical water splitting is attractive to solve the energy and environment problems by using abundant sunlight as clean power source and producing H_2 as a carbon-free fuel product.[1,2] This task, however, is challenging due to water splitting is an uphill reaction with a Gibbs free energy change of $\Delta G = +237.2$ KJ/mol, which equals to 1.23 eV per electron transferred.[3] While wide band-gap semiconductors, such as TiO_2, $SrTiO_3$, $BiVO_4$ and TaON are inefficient in utilizing the visible-light energy,[4-7] narrow band-gap semiconductors are generally suffered from improper band positions, and therefore require large amount external electric power to assist the overall water splitting reaction.[3,4] For example, Si (E_g=1.12 eV) and α-Fe₂O₃ (E_g=2.0 eV), though effectively absorb visible light, are abundantly available and environmentally nontoxic, can only perform water splitting with large applied external voltages.[8-14] The valence band position (E_{vb}) of Si is higher than the oxygen evolution reaction (OER) potential and therefore not suitable for water oxidation. Furthermore, Si easily forms insulating oxides at its surface in electrolyte, especially at positive potentials for water oxidation, which will impede the charge transferring across the Si/electrolyte interface.[13-17] Although α-Fe₂O₃ is stable in electrolyte and owns a suitable band-gap, it has a conduction band potential (E_{cb})

below the hydrogen evolution reaction (HER) potential.[8] These drawbacks may be partially compensated by hybridizing Si and α-Fe₂O₃ into a heterogeneous photoelectrode. Through material hybridization, the charge carriers responsible for the HER and OER can be derived from different catalytic materials,[18-20] and enlarged photovoltage can be cooperatively provided by these components.[19,20] Moreover, the heterojunctions can also endow the photoelectrodes with synergistic effects such as enhanced electron-hole separation and collection.[20-22]

Apart from the thermodynamic requirements, the charge transport in a high-performance photoelectrode should also be efficient, so as to ensure the collection of the photogenerated carriers.[4] In this regard, α-Fe₂O₃ is disadvantaged due to its poor conductivity,[23] short photogenerated carrier lifetime,[24] and a very short hole diffusion length (L_D, 2-4 nm) as compared to its long light penetrating length ($α^{-1}$, on the order of 100nm).[25] Although considerable progress has been made by doping,[26,27] the state-of-the-art performance of α-Fe₂O₃ is still low with small photocurrents. Other strategies include morphological nanostructuring[28-31] and coupling of α-Fe₂O₃ with nanostructured materials with high conductivities,[32] by which the charge collection length can be shortened while the light absorption could be simultaneously maintained. In this respect, Si nanowire

array is a potential candidate, as it prolongs the light absorbing length in the axial direction and shortens the carrier collection distance in the radial direction.[10,11] Combined with the excellent conductivity of Si, this merit makes Si nanowire array a promising material for a favorable structural support and charge collector in a Si/α-Fe$_2$O$_3$ hybrid photoelectrode.

To date, considerable efforts have been made to maximize the photogenerated charge transfer from the photoelectrodes to the electrolyte by controlling the sizes of the constituent materials of photoelectrodes. However, the relationships between the sizes of the components in composite photoelectrodes and the energy band positions of the components, as well as the material-size-related charge transfer processes at hetero junctions remain unclear. Given that the energy band bending in a semiconductor in contact with an electrolyte could be very abnormal if the size of the semiconductor shrink to so small that the semiconductor is fully depleted from major carriers, insights into the material-size-related energy band positions, band bending and charge transfer in a composite photoelectrode are highly desired for the design and optimization of composite photoelectrodes or photocatalysts for water splitting.

In this work, we report a photoanode consisting of n-Si/α-Fe$_2$O$_3$ core/shell nanowire arrays readily prepared through thermal decomposition of Fe(NO$_3$)$_3$ on chemically etched Si nanowires. The impact of the thickness of the α-Fe$_2$O$_3$ shell on the photoelectrochemical performance of the present photoanode was investigated in detail. Towards photoelectrochemical water splitting, this hybrid photoanode exhibited a low photocurrent onset potential and a high photocurrent, as well as fine stability, under simulated AM 1.5 G irradiation.

Experimental section

Preparation of the n-Si nanowire arrays

The Si nanowires (SiNWs) were fabricated by a modified Peng's method.[33] Briefly, single crystalline n-Si (100) wafers (2-4 Ωcm) were cut into rectangular slices of 1cm×2cm and the slices were cleaned by ultrasonic in acetone and distilled water successively. The cleaned silicon slices were immersed into a solution containing 5 mM AgNO$_3$ and 4.8 M HF to deposit Ag particles, which would act as catalyst in the following etching process. Subsequently, the silicon with Ag particles were etched in an aqueous solution of 4 mM H$_2$O$_2$ and 4.8 M HF at 50℃ for 5 min, 10 min and 20 min to produce the n-Si nanowire arrays with different lengths. Finally, after removing the residual Ag particles by immersing the n-Si into aqua fortis for an hour, n-Si nanowire arrays were formed on the n-Si substrate.

Preparation of n-Si/α-Fe$_2$O$_3$ core/shell nanowire arrays

To sheathe the SiNWs with an α-Fe$_2$O$_3$ layer, the SiNWs were first treated in a 5% HF solution to remove the oxide layer and then immersed into a stirring Fe(NO$_3$)$_3$ ethanol solution for 3 min. After that, the SiNWs were immediately transferred into a tubular furnace for the subsequent thermal decomposition of the Fe(NO$_3$)$_3$ at 500°C for 3 hours under N$_2$ atmosphere. We denoted the sample prepared with X mM Fe(NO$_3$)$_3$ as n-Si/α-Fe$_2$O$_3$-XmM.

Fabrication of the electrodes

For the electrochemical and photoelectrochemical measurements, In-Ga eutectics were rubbed on the back sides of the silicon slices with the n-Si/α-Fe$_2$O$_3$ core/shell nanowire arrays to obtain ohmic contacts. Then Cu foils were coated on the In-Ga eutectics and used as external connections. The whole backsides and edges of the samples were isolated from the electrolyte by sealing with epoxy. The active

electrode areas for measurements in the front side were also defined by epoxy.

Electrochemical and photoelectrochemical characterization

Photoelectrochemical properties of the n-Si/α-Fe$_2$O$_3$ core/shell nanowire arrays were investigated in a three-electrode cell. The as-prepared nanowires were used as the working electrode and a Pt foil was used as the counter electrode. A standard saturated calomel electrode (SCE) was used as the reference electrode. The measured potentials against SCE were converted to reversible hydrogen electrode (RHE) scale according to the Nernst equation

$$E_{RHE}=E_{SCE}+0.059\text{pH}+E^0_{SCE}$$

Wherein E_{RHE} is the converted potentials vs RHE, E_{SCE} is the potential of SCE and is 0.242V at 25℃, E_{SCE} is the experimentally measured potential against SCE. An aqueous solution of 1 M NaOH (pH=13.8) was used as the electrolyte. A light with constant intensity of 100 mW/cm^2 from a 500W Xe lamp passed through an AM 1.5G filter was employed as the irradiation source.

Mott-Schottky measurements were performed on α-Fe$_2$O$_3$ film prepared on FTO glass substrate (α-Fe$_2$O$_3$/FTO) and n-Si/α-Fe$_2$O$_3$ core/shell nanowire arrays in 1 M NaOH in dark in the same three-electrode cell for the photoelectrochemical measurements.

Results and discussion

Preparation of n-Si/α-Fe$_2$O$_3$ core/shell nanowire arrays
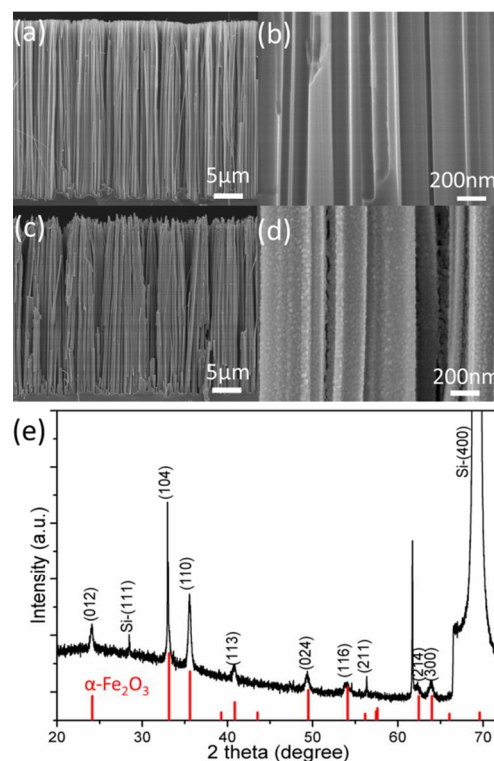
Fig. 1 SEM images of SiNWs with an etching time of 20 min (a) (b), and α-Fe$_2$O$_3$ coated SiNWs prepared with 200 mM Fe(NO$_3$)$_3$ (c) (d); (e) XRD spectra of α-Fe$_2$O$_3$ coated SiNWs prepared with 200 mM Fe(NO$_3$)$_3$; Red lines highlight the diffraction peaks of α-Fe$_2$O$_3$ (JCPDS 33-0664).

Figure 1a, b shows the typical scanning electron microscopy (SEM) images of the Si nanowire (SiNWs) prepared by chemical etching.[33]

More SEM images of the SiNWs could be seen in Figure S1. These nanowires are well aligned and perpendicular to the substrate with diameters of 40-400 nm. The n-Si/α-Fe$_2$O$_3$ core/shell nanowire arrays were prepared through thermal decomposition of Fe(NO$_3$)$_3$ on chemically etched SiNWs. We denoted the sample prepared with X mM Fe(NO$_3$)$_3$ as n-Si/α-Fe$_2$O$_3$-XmM. The representative SEM images of the n-Si/α-Fe$_2$O$_3$-200mM are shown in Figure 1c, d. As can be observed, after the α-Fe$_2$O$_3$ modification the sample retained the basal morphology of the SiNWs except for the noticeable rougher surface. The X–ray diffraction (XRD) patterns shown in Figure 1e clearly demonstrate the formation of α-Fe$_2$O$_3$ (hematite, JCPDS 33-0664) in the product. The unindexed peak at 61.7 degree could be assigned to the diffraction of the Cu k-beta ray ($\lambda_{k\beta}$=0.1392 nm) by the Si (400) planes.
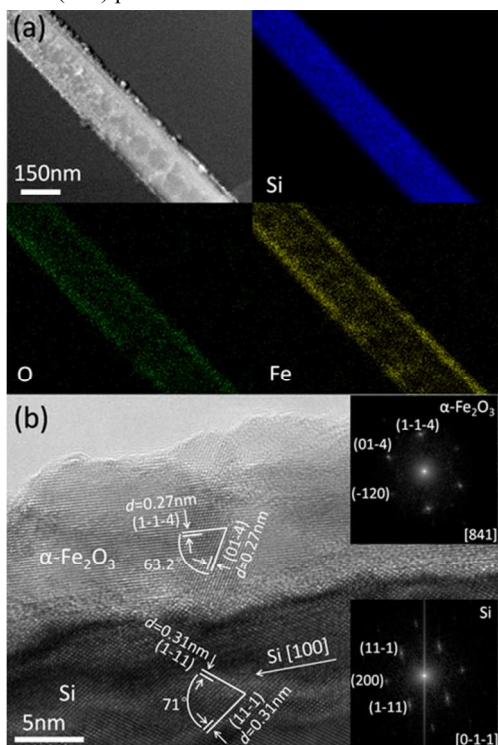
Fig. 2 (a) STEM image and EDX elemental mapping of an n-Si/α-Fe$_2$O$_3$ core/shell nanowire prepared with 100 mM Fe(NO$_3$)$_3$; (b) HRTEM image of an n-Si/α-Fe$_2$O$_3$ core/shell nanowire prepared with 20 mM Fe(NO$_3$)$_3$; insets are the corresponding indexed FFT patterns of α-Fe$_2$O$_3$ (upper right) and Si (lower right).

The composition of the product was further analyzed by a scan transmission electron microscopy (STEM) equipped with an energy–dispersive X–ray spectroscopy (EDX) facility. Figure 2a shows a typical dark-field STEM image of a nanowire and its corresponding elemental mapping. It can be found that the Si signal distributes homogeneously in the core region, while the Fe and O elements mainly exist at the outside layer of the nanowire. A full EDX spectrum was provided in Figure S2a. N element, which could be a possible doping impurity, was not found in the product, as was confirmed by the X-ray photoelectron spectroscopy (XPS) (Figure S2b). The intrinsic crystal structure of the core/shell Si/α-Fe$_2$O$_3$ nanowires was further characterized by the high-resolution TEM (HRTEM). In Figure 2b, the inter-planar distances of 0.27 nm in the shell region match well with the lattice fringes of (1-1-4) and (01-4) planes of α-Fe$_2$O$_3$. In the core region, the labeled d-spacings are consistent with the lattice planes of Si. In HRTEM observation, we observed that the thickness of the the α-Fe$_2$O$_3$ shell is not very uniform in different nanowires and at different regions of individual

nanowires. This could be attributed to the fact that the void and the distances among the n-Si nanowires obtained from chemical etching were not uniformly controlled, which hindered the uniformity of the α-Fe$_2$O$_3$ shell. The thickness of the α-Fe$_2$O$_3$ in most n-Si/α-Fe$_2$O$_3$-20mM nanowires is less than 9 nm, under TEM observations. Based on the XRD, EDX mapping and HRTEM analyses, a core/shell configuration of the as-prepared n-Si/α-Fe$_2$O$_3$ nanowires can thereby be confirmed.

Photoelectrochemical and electrochemical characterization

The linear scan voltammograms (LSVs) of the n-Si/α-Fe$_2$O$_3$-20mM nanowire arrays with different nanowire lengths are presented in Figure 3. As can be seen, all the three samples exhibited small dark currents and remarkable photoresponse upon illumination. By contrast, α-Fe$_2$O$_3$ film prepared on FTO glass, p-Si nanowire array and planar silicon wafer substrate, showed very poor photoresponse (Figure S3, S4). We also performed the photoelectrochemical test on SiNWs without α-Fe$_2$O$_3$ modification, which exhibited very small (less than 0.1 mA/cm^2) and instable currents in the 1 M NaOH electrolyte, as can be seen in Figure S5. The onset potentials of photocurrents are located at about 0.5 V vs RHE, where obvious photoresponse can be observed. It is worthwhile to note that the onset potential is several hundred mV more cathodic than that of single silicon or doped α-Fe$_2$O$_3$ photoanode even after surface catalyst modification,[12,13,15,34-37] indicating that smaller external voltage is required for water splitting on the present n-Si/α-Fe$_2$O$_3$ photoanode. The photocurrent enhanced with increasing length of the n-Si/α-Fe$_2$O$_3$ nanowires, which is consistent with the results in n-Si/n-TiO$_2$ nanowire photoanodes and may be due to the increased light absorption as well as the enlarged electrode/electrolyte contact area in the longer nanowires.[20] The n-Si/α-Fe$_2$O$_3$-20mM with a length of about 25μm showed a high photocurrent of 5.28 mA/cm^2 at 1.23 V vs RHE, which is much larger that of α-Fe$_2$O$_3$ photoanodes.[8] In comparison with silicon-based hybrid photoanode such as n-Si/n-TiO$_2$, n-Si/n-ZnO and n-Si/InGaN, the present n-Si/α-Fe$_2$O$_3$ photoanode also exhibited a much greater photocurrent,[20,38,39] which could be attributed to the superior photoactivity of α-Fe$_2$O$_3$ in the visible-light region.
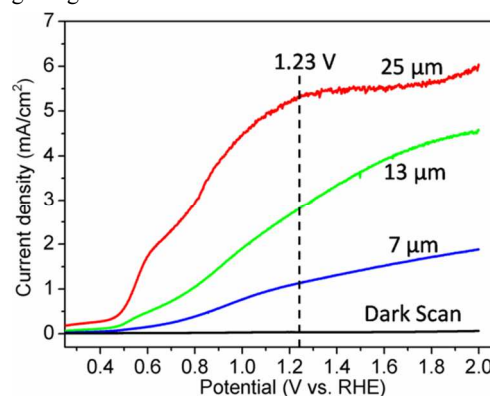
Fig. 3 Linear scan voltammograms (LSVs) of the n-Si/α-Fe$_2$O$_3$-20mM with lengths of 7 μm, 13μm and 25μm. Measurements were performed with a scan rate of 50 mV/s, in 1 M NaOH electrolyte under simulated AM 1.5G illumination of 100 mW/cm^2.

To determine the working mechanism of the n-Si/α-Fe$_2$O$_3$ core/shell nanowire array photoanodes, the energy band diagram of the Si/α-Fe$_2$O$_3$/electrolyte junction was roughly constructed based on the existing energy band data of the n-Si and α-Fe$_2$O$_3$ reported in literatures,[42,43] (Detailed energy band data and the diagram are available in Figure S6). An n/n junction forms at the n-Si/α-Fe$_2$O$_3$ interface, which seems similar to the n-Si/n-TiO$_2$ junction.[20] However, an accurate knowledge of the α-Fe$_2$O$_3$/electrolyte junction

requires the electrochemical properties of the α-Fe$_2$O$_3$. The energy band edges of the α-Fe$_2$O$_3$ relative to the water splitting reaction potentials, the charge carrier densities and the space charge region width of the α-Fe$_2$O$_3$, which can be very different when different preparation methods and surface treatments process are used. To obtain the electrochemical properties of the α-Fe$_2$O$_3$, we performed electrochemical impedance measurements on the α-Fe$_2$O$_3$ film prepared on FTO glass substrate through the same procedure. The conducting type, carrier density and flatband potential of the α-Fe$_2$O$_3$ were determined using the Mott-Schottky equation[40]

$$1/C^2 = (2/e_0\varepsilon\varepsilon_0 N_d)[(V-V_{FB})-kT/e_0]$$

wherein e_0 is the electron charge, ε is the dielectric constant of α-Fe$_2$O$_3$, ε_0 is the permittivity of vacuum, N_d is the dopant density, V is the electrode potential, V_{FB} is the flatband potential, T is the temperature and k is Boltzmann's constant. The Mott-Schottky plot collected from the α-Fe$_2$O$_3$/FTO is presented in Figure 4a. The positive slope indicates that the α-Fe$_2$O$_3$ is an n-type semiconductor. By extrapolating the X intercept, the V_{FB} of the α-Fe$_2$O$_3$ is determined to be 0.26 V vs RHE.

The electron density of the α-Fe$_2$O$_3$ can also be calculated from the slope of the Mott-Schottky plot.[40, 41]

$$N_d = (2/e_0\varepsilon\varepsilon_0)[d(1/C^2)/dV]^{-1}$$

With an ε of 80, the electron density is calculated to be 3.31×10^{19}cm^{-3}, which is comparable to the typical values for α-Fe$_2$O$_3$.[36] The depletion width (W) of the α-Fe$_2$O$_3$ in contact with the electrolyte was roughly inferred to be 16.1 nm from the following equation[40]

$$W = [2\varepsilon\varepsilon_0(V-V_{FB})/e_0 N_d]^{1/2}$$

Wherein V is the Fermi level of the electrolyte and is chosen close to the water oxidation potential, 1.23 V vs RHE.
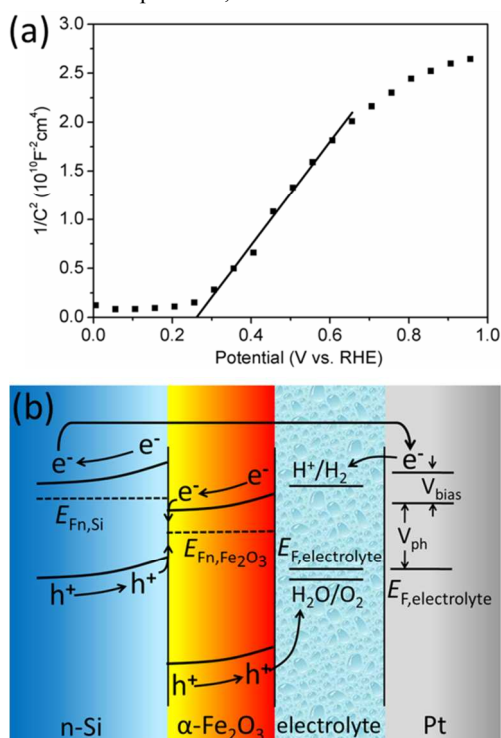
Fig. 4 (a) Mott-Schottky plot of α-Fe$_2$O$_3$ on FTO measured at a frequency of 10 kHz in 1M NaOH in dark. (b) Schematic energy diagram of and

charge transfer in n-Si/α-Fe$_2$O$_3$ in contact with electrolyte under illumination.

Since the mean thickness of the α-Fe$_2$O$_3$ (less than 9 nm in Si/α-Fe$_2$O$_3$-20mM sample) is smaller than the calculated depletion width (16.1nm) for bulk α-Fe$_2$O$_3$, the α-Fe$_2$O$_3$ shell will be completely depleted from electrons and a resultant internal field will exist everywhere in the α-Fe$_2$O$_3$, which would be beneficial to the charge collection in the α-Fe$_2$O$_3$. The energy band diagram is sketched in Figure 4b. This condition is quite different from those previously reported n/n junctions such as n-Si/n-TiO$_2$ and Si/α-Fe$_2$O$_3$, where relative thick TiO$_2$ or α-Fe$_2$O$_3$ was used and part of the TiO$_2$ or α-Fe$_2$O$_3$ may still be in a field-free region.[20,22] Charge transfer in field-free region of α-Fe$_2$O$_3$ will promote recombination loss due to the very short hole diffusion length (L_D, 2-4 nm) and short photogenerated carrier lifetime for α-Fe$_2$O$_3$.[8,24,25] Upon illumination, the band bending facilitates the separation and collection of the photogenerated electrons in the Si and the holes in the α-Fe$_2$O$_3$, which initiate the water reduction and oxidation reaction, respectively. The photogenerated electrons in the α-Fe$_2$O$_3$ and holes in the Si will be transferred towards the interface of n-Si/α-Fe$_2$O$_3$ by the internal fields and recombined there.[22] Such recombination process is crucial to achieving the "Z-scheme" water splitting.[18] The photovoltage (V_{ph}) is the sum of photovoltage of the Si and the α-Fe$_2$O$_3$, which is equal to the difference of the quasi Fermi level of electron in Si ($E_{Fn,Si}$ in Figure 4b) and the Fermi level of the electrolyte ($E_{F,electrolyte}$). Thus, V_{ph} can be expressed as $V_{ph}(total)=V_{ph}(Si/\alpha\text{-Fe}_2O_3)+V_{ph}(Fe_2O_3/electrolyte)$.[20] Accordingly, the photovoltage in this hybrid photoanode is greater than individual Si or α-Fe$_2$O$_3$ photoanode. This is why smaller external voltage is required for the n-Si/α-Fe$_2$O$_3$ photoanode and the photoresponse starts at a less positive potential.

Since the feature size of α-Fe$_2$O$_3$ is critical to its photoelectrochemical performance,[30] and also may have an effect on the band edge position of the n-Si core, the impact of the α-Fe$_2$O$_3$ thickness on the overall performances of the photoanode is further investigated. By increasing the concentration of the Fe(NO$_3$)$_3$ in ethanol solution, the mean thickness of α-Fe$_2$O$_3$ is increased from approximate 7.5 nm (estimated from TEM observations) in the n-Si/α-Fe$_2$O$_3$-20mM to more than 50 nm in the n-Si/α-Fe$_2$O$_3$-200mM. The thicknesses of the α-Fe$_2$O$_3$ in samples prepared with Fe(NO$_3$)$_3$ concentrations less than 20 mM cannot be accurately measured.
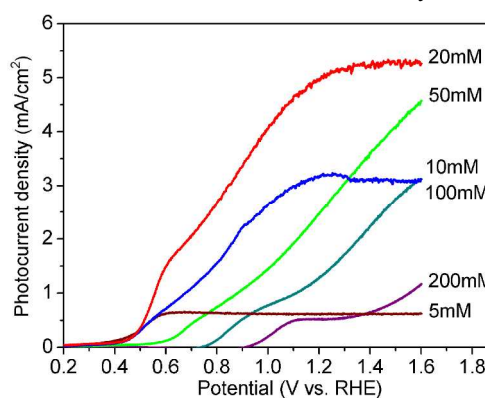
Fig. 5 Linear scan voltammograms of n-Si/α-Fe$_2$O$_3$ prepared with Fe(NO$_3$)$_3$ concentrations from 5 mM to 200 mM. Measurements were performed with a scan rate of 50 mV/s, in 1 M NaOH electrolyte under simulated AM 1.5G illumination of 100 mW/cm^2.

Figure 5 compares the LSVs of the n-Si/α-Fe$_2$O$_3$ photoanodes with various thicknesses of α-Fe$_2$O$_3$. It can be observed that the n-Si/α-Fe$_2$O$_3$-20mM exhibited the highest performance with a plateau photocurrent of 5.28 mA/cm^2 and an onset potential of 0.5 V vs

RHE. In other samples, smaller photocurrents were observed. The decreased photocurrents in samples with thicker α-Fe$_2$O$_3$ may be due to the deteriorated charge collection in the α-Fe$_2$O$_3$, since that α-Fe$_2$O$_3$ has a very short hole diffusion length (L_D, 2-4 nm) and short photogenerated carrier lifetime,[24,25] and therefore charge collection in thicker α-Fe$_2$O$_3$ is accompanied with larger recombination loss and greater potential drop.[8] In thicker α-Fe$_2$O$_3$, a large fraction of the incident photons were wasted in the inner region of the α-Fe$_2$O$_3$, i.e., in the region far from the α-Fe$_2$O$_3$/electrolyte interface, where the excited electron-hole pairs could be lost through bulk recombination.[8] The harvestless light absorption in the inner region of the α-Fe$_2$O$_3$ will affect the productive light absorption in the surface region of α-Fe$_2$O$_3$, as the incident light could be reflected back and forth between the nanowires. In addition, as the α-Fe$_2$O$_3$ is poor in electronic conducting, charge transport in thicker α-Fe$_2$O$_3$ brings greater potential drop.[8] This could be observed from the LSVs of the samples. The LSVs of the samples with thin α-Fe$_2$O$_3$, i.e. Si/α-Fe$_2$O$_3$-20mM, Si/α-Fe$_2$O$_3$-10mM and Si/α-Fe$_2$O$_3$-5mM, showed a plateau at moderately positive potentials; however, the LSVs of the samples with thick α-Fe$_2$O$_3$ did not show a similar plateau even at potentials beyond 1.5 V. The photocurrents were also decreased when the thickness of the α-Fe$_2$O$_3$ were further decreased, as shown in n-Si/α-Fe$_2$O$_3$-10mM and n-Si/α-Fe$_2$O$_3$-5mM samples. This reduction of the photocurrent could be resulted from the limited light absorption in the extremely thin α-Fe$_2$O$_3$. The smaller photocurrents observed on the samples with thinner α-Fe$_2$O$_3$ also suggest that the photocurrents do not come from silicon etching by the electrolyte.

It should also be noted that the photocurrent onset potential shifted to a less positive direction as the α-Fe$_2$O$_3$ thickness is decreased. The onset potential for the sample with the thickest α-Fe$_2$O$_3$ shell, i.e., n-Si/α-Fe$_2$O$_3$-200mM, is 0.93 V (vs RHE). When the thickness of the α-Fe$_2$O$_3$ was decreased, as in n-Si/α-Fe$_2$O$_3$-20mM, the onset potential shifted to 0.5 V (vs RHE). The onset potential of photocurrent on a photoelectrode is commonly concerned with the photogenerated voltage and the band edge positions of the semiconductors.[4] Since the decrease in the thickness of α-Fe$_2$O$_3$ should not generate a larger photovoltage in principle, it is then considered that the shift of the onset potential may be related to movement of the band edge positions of the n-Si, in which the electrons are responsible for the water reduction half reaction. The quasi-fermi level of the electrons in the light-irradiated n-Si ($E_{Fn,Si}$ in Figure 4b) is one of the key factors that decide how much external voltage is required to complete the water splitting reaction and where the photocurrent onset potential should be located.

Impact of the α-Fe$_2$O$_3$ thickness on the energy band positions of the n-Si

To reveal the impact of the α-Fe$_2$O$_3$ shell thickness on the energy band positions of n-Si, the flatband potentials of the n-Si ($V_{FB,Si}$) in various n-Si/α-Fe$_2$O$_3$ samples were measured through Mott-Schottky analyses. It seems infeasible because there are two depletion layers existing in series in this hybrid photoanode, the depletion layer in the Si and the depletion layer in the α-Fe$_2$O$_3$. The total capacitance can be expressed as

$$1/C_{total} = 1/C_{Si} + 1/C_{Fe2O3}$$

However, it can be seen from the Mott-Schottky equation

$$1/C^2 = (2/e_0\varepsilon\varepsilon_0 N_d)[(V - V_{FB}) - kT/e_0]$$

that $1/C$ is proportional to $1/N_d^{1/2}$. We notice that the N_d of the phosphorus doped Si wafer (2-4 Ωcm), 1.52×10^{15} cm^{-3}, is very small compared to the measured N_d of the α-Fe$_2$O$_3$ (3.31×10^{19} cm^{-3}). Therefore, $1/C_{Fe2O3}$ is negligibly small relative to the $1/C_{Si}$. It can be

expected that the C_{total} may be mainly governed by the Si, and a Mott-Schottky measurement of the Si/α-Fe$_2$O$_3$ may mainly reflect the electronic information of Si. In order to verify our assumption, we performed Mott-Schottky test on Si/α-Fe$_2$O$_3$ samples with Si with different conduction type. A negative and positive slope in Mott-Schottky plot should be observed from a p-type and n-type semiconductor, respectively. Mott-Schottky plots of the Si/α-Fe$_2$O$_3$ with p-type and n-type Si are presented in Figure 6 a, b. The negative and positive slope of the Mott-Schottky plots from p-Si/α-Fe$_2$O$_3$ and n-Si/α-Fe$_2$O$_3$ confirm that the capacitance of the Si/α-Fe$_2$O$_3$ is mainly governed by the depletion layer in the Si. The N_d calculated from Mott-Schottky plot of n-Si/α-Fe$_2$O$_3$-20mM is 1.08×10^{16} cm^{-3}, which is close to that of the Silicon wafer we used, 1.52×10^{15} cm^{-3}. Considering the cylindrical geometry of the Si nanowires, the deviation is reasonable. The result further conformed that Mott-Schottky test performed on the n-Si/α-Fe$_2$O$_3$ product could be used to reveal the electronic information of the n-Si.
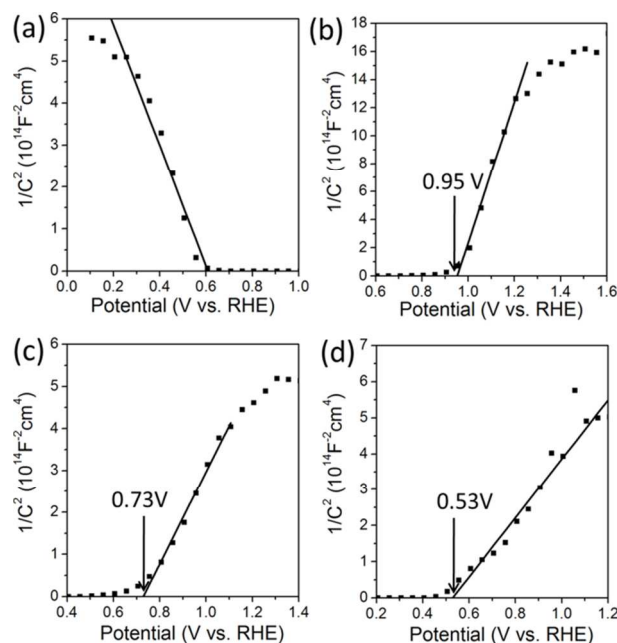
Fig. 6 (a) Mott-Schottky plot from (a) p-Si/α-Fe$_2$O$_3$-20mM with p-type Si (2-4 Ωcm), (b) n-Si/α-Fe$_2$O$_3$-200mM, (c) n-Si/α-Fe$_2$O$_3$-20mM and (d) n-Si/α-Fe$_2$O$_3$-5mM, measured at a frequency of 50 kHz in 1 M NaOH in dark.

The Mott-Schottky plots of the n-Si/α-Fe$_2$O$_3$ with various α-Fe$_2$O$_3$ thicknesses are presented in Figure 6 (b-d). By extrapolating the X intercept, the flat band potential of the Si core, $V_{FB,Si}$, could be inferred. It is interesting that the photocurrent onset potential is more negative than the measured flat band potential of the n-Si. This is because that the flat band potential of the n-Si is measured in the dark, while the photocurrent onset is observed when the photoanode is under illumination. Under illumination, the energy band bending of the α-Fe$_2$O$_3$ decreases, and thus the energy bands of the n-Si moves upwards. This is illustrated in Figure S7. Notably, the flat band potential of Si shifted to cathodic direction as the α-Fe$_2$O$_3$ thickness was decreased (Figure 6 b-d). The $V_{FB,Si}$ moved from 0.95 V (vs RHE) in n-Si/α-Fe$_2$O$_3$-200mM to 0.73 V (vs RHE) in n-Si/α-Fe$_2$O$_3$-20mM and to 0.53 V (vs RHE) in n-Si/α-Fe$_2$O$_3$-5mM. The upward shift of the $V_{FB,Si}$ suggests that the band edge positions of the n-Si are higher in samples with thinner α-Fe$_2$O$_3$. The elevated energy bands of Si could provide more energetic photogenerated electrons for water reduction, which would result in possible less positive photocurrent onset potentials.

To understand the effect of the α-Fe$_2$O$_3$ thickness on the energy band edge positions of the n-Si, we calculated the electric field strength and the band bending in the n-Si/α-Fe$_2$O$_3$/electrolyte junction. Assuming that the energy band offsets at the n-Si/α-Fe$_2$O$_3$ interface are constant, which is the case in the Anderson band model, the band edge positions of Si at the n-Si/α-Fe$_2$O$_3$ interface are dependent on the potential drop in the depletion layer of the α-Fe$_2$O$_3$, as can be seen in the energy diagram in Figure 4b. For a bulk semiconductor in contact with an electrolyte, the potential drop within the semiconductor is constant and is the same as the difference between the V_{FB} of the semiconductor and the E_F of the electrolyte. However, the potential drop in a semiconductor will be closely related to its feature size when the size of the semiconductor is smaller than the width of the depletion layer in bulk.[44] For example, the potential drop in spherical nanoparticles completely depleted of major charge carriers was found to be very small compared to that in the bulk.[45]

In our case, supposing that the α-Fe$_2$O$_3$ shell is sufficiently thin relative to the mean diameter of the nanowires, the potential drop in the α-Fe$_2$O$_3$ was calculated by relating the charge density distribution (see Figure S8a) and the electric field strength (see Figure S8b) in the n-Si/α-Fe$_2$O$_3$ junction as embodied by the Poisson equation (The calculation is provided in the Supporting Information). The dependence of the potential drop in the α-Fe$_2$O$_3$ on its depletion layer width, i.e., its thickness, can be expressed as

$$V_{Fe2O3} = (e_0 N_d/2\varepsilon\varepsilon_0)d^2 + (e_0 N_{Si}W_{Si}/\varepsilon\varepsilon_0)d \quad (0 \cong d \cong W)$$

Where d is the thickness of the α-Fe$_2$O$_3$, W is the depletion layer width for bulk α-Fe$_2$O$_3$ in contact with the electrolyte and in the same condition, N_{Si} is the dopant density of the n-Si, W_{Si} is the width of the depletion layer in the n-Si and V_{Fe2O3} is the potential drop in the α-Fe$_2$O$_3$ with a thickness of d. The first term in right part of the expression is in the same form as the potential drop in the depletion layer of a single semiconductor in contact with an electrolyte,[46] and can be assigned to the positive charge in the depleted α-Fe$_2$O$_3$ and the corresponding negative charge transferred from the α-Fe$_2$O$_3$ to the electrolyte. The second term takes the form of the potential drop between two plates of a parallel plate capacitor and can be attributed to the positive charge in the depletion layer of the n-Si and the corresponding negative charge transferred from the n-Si to the electrolyte. According to the above expression, the potential drop in a thinner α-Fe$_2$O$_3$ should be smaller than that in a thicker one. As the Si is contact with the α-Fe$_2$O$_3$, a smaller potential drop in a thinner α-Fe$_2$O$_3$ will give higher band positions for the Si. The impact of the α-Fe$_2$O$_3$ thickness on the energy diagram of the n-Si/α-Fe$_2$O$_3$/electrolyte junction is illustrated in Figure S9. Then, the onset potential of Si/α-Fe$_2$O$_3$ with thinner α-Fe$_2$O$_3$ shells shifted to the less positive direction.

Since Si is not stable in aqueous solution, especially at anodic potentials for water oxidation, the stabilities of Si-based photoanodes are often problematic. The photocurrent of SiNWs without α-Fe$_2$O$_3$ modification quickly decreased to smaller than 0.1 mA/cm^2 at 1.23 V vs RHE after five LSV scans (see Figure S5). By contrast, the n-Si/α-Fe$_2$O$_3$-20mM retained a photocurrent larger than 1.7 mA/cm^2 after working for 3 hours (Figure S10), demonstrating the protective role of the α-Fe$_2$O$_3$ shell. Compared with Pt and carbon protected Si photoelectrodes, the present photoanodes showed superior performance in stability.[17]

Conclusions

In conclusion, we have fabricated a high-performance n-Si/α-Fe$_2$O$_3$ core/shell nanowire array photoanode toward photoelectrochemical water splitting. Photocurrent of the sample with optimized α-Fe$_2$O$_3$ thickness started at 0.5 V vs RHE, which is several hundred mV lower than those of reported n-Si or α-Fe$_2$O$_3$ photoanodes. A high photocurrent of 5.28 mA/cm^2 at 1.23 V vs RHE, which is larger than most of those observed on α-Fe$_2$O$_3$, was also achieved. It is found that the thickness of α-Fe$_2$O$_3$ has a strong effect on the photocurrent onset potential of the n-Si/α-Fe$_2$O$_3$ core/shell nanowire photoanodes. Mott-Schottky measurements and energy band calculation suggest that the band positions of the Si are elevated as the α-Fe$_2$O$_3$ thickness is decreased. The α-Fe$_2$O$_3$ shell with an optimized thickness is favorable for locating the energy bands of Si at a relatively high level and maximizing the charge collection in α-Fe$_2$O$_3$, and thus achieving the low photocurrent onset potential and the high photocurrent. This work represents a novel approach to achieving high-performance photoelectrode with visible-light absorbing semiconductors through heterogeneous photocatalyst design and size-related optimization. It is expected that this work will shed some new light on the preparation of cost-effective, environment friendly and high-performance photocatalyst for fuel production and pollutant degradation.

ASSOCIATED CONTENT

Supporting Information. SEM images of Si nanowires with different lengths, EDS, XPS and energy band data of n-Si/α-Fe$_2$O$_3$, electrochemical and photoelectrochemical performance of α-Fe$_2$O$_3$ film on FTO, cauculation of potential drop in α-Fe$_2$O$_3$, and stability test of the SiNWs and the n-Si/α-Fe$_2$O$_3$ photoanodes. This material is available free of charge via the Internet at http://pubs.acs.org.

Notes and references

^{a} Key Laboratory of Photochemical Conversion and Optoelectronic Materials, Technical Institute of Physics and Chemistry, Chinese Academy of Sciences, Beijing, 100190, P. R. China; Tel/Fax: 86-10-82543513; E-mail: shegw@mail.ipc.ac.cn, shiws@mail.ipc.ac.cn
^{b} General Research Institute for Nonferrous Metals, Beijing, 100088, China.

† Electronic Supplementary Information (ESI) available: SEM images of Si nanowires with different lengths, EDS, XPS and energy band data of n-Si/α-Fe$_2$O$_3$, electrochemical and photoelectrochemical performance of α-Fe$_2$O$_3$ film on FTO, cauculation of potential drop in α-Fe$_2$O$_3$, stability test of the SiNWs and the n-Si/α-Fe$_2$O$_3$ photoanodes, and discussions on the mass transport in the n-Si/α-Fe$_2$O$_3$ core/shell nanowires.

1 M. Gratzel, *Nature,* 2001, **414,** 338-344.
2 J. Bard and M. A. Fox, *Acc. Chem. Res.,* 1995, **28,** 141-145.
3 A. Kudo and Y. Miseki, *Chem. Soc. Rev.,* 2009, **38,** 253-278.
4 M. G. Walter, E. L. Warren, J. R. McKone, S. W. Boettcher, Q. Mi, E. A. Santori and N. S. Lewis, *Chem. Rev.,* 2010, **110,** 6446-6473.
5 A. Fujishima and K. Honda, *Nature,* 1972, **238,** 37-38.
6 Q. X. Jia, K. Iwashina and A. Kudo, *Proc. Natl. Acad. Sci. U.S.A.,* 2012, **109,** 11564-11569.

7   M. Higashi, R. Abe, A. Ishikawa, T. Takata, B. Ohtani and K. Domen, *Chem. Lett.,* 2008, **37,** 138-139.

8   K. Sivula, F. Le Formal and M. Graetzel, *Chemsuschem,* 2011, **4,** 432-449.

9   S. Y. Reece, J. A. Hamel, K. Sung, T. D. Jarvi, A. J. Esswein, J. J. H. Pijpers and D. G. Nocera, *Science,* 2011, **334,** 645-648.

10 S. W. Boettcher, J. M. Spurgeon, M. C. Putnam, E. L. Warren, D. B. Turner-Evans, M. D. Kelzenberg, J. R. Maiolo, H. A. Atwater and N. S. Lewis, *Science,* 2010, **327,** 185-187.

11 M. D. Kelzenberg, S. W. Boettcher, J. A. Petykiewicz, D. B. Turner-Evans, M. C. Putnam, E. L. Warren, J. M. Spurgeon, R. M. Briggs, N. S. Lewis and H. A. Atwater, *Nat. Mater.,* 2010, **9,** 239-244.

12 K. Jun, Y. S. Lee, T. Buonassisi and J. M. Jacobson, *Angew. Chem., Int. Ed.,* 2012, **51,** 423-427.

13 Y. W. Chen, J. D. Prange, S. Duehnen, Y. Park, M. Gunji, C. E. D. Chidsey and P. C. McIntyre, *Nat. Mater.,* 2011, **10,** 539-544.

14 K. Q. Peng, X. Wang, X. L. Wu and S. T. Lee, *Nano Lett.,* 2009, **9,** 3704-3709.

15 K. Sun, N. Park, Z. Sun, J. Zhou, J. Wang, X. Pang, S. Shen, S. Y. Noh, Y. Jing, S. Jin, P. K. L. Yu and D. Wang, *Energ Environ. Sci.,* 2012, **5,** 7872-7877.

16 K. Q. Peng and S. T. Lee, *Adv. Mater.,* 2011, **23,** 198-215.

17 X. Wang, K. Q. Peng, X. J. Pan, X. Chen, Y. Yang, L. Li, X. M. Meng, W. J. Zhang and S. T. Lee, *Angew. Chem., Int. Ed.,* 2011, **50,** 9861-9865.

18 H. Tada, T. Mitsui, T. Kiyonaga, T. Akita and K. Tanaka, *Nat. Mater.,* 2006, **5,** 782-786.

19 Khaselev and J. A. Turner, *Science,* 1998, **280,** 425-427.

20 Y. J. Hwang, A. Boukai and P. Yang, *Nano Lett.,* 2009, **9,** 410-415.

21 X. Qi, G. She, Y. Liu, L. Mu and W. Shi, *Chem. Commun.,* 2012, **48,** 242-244.

22 M. T. Mayer, C. Du and D. Wang, *J. Am. Chem. Soc.,* 2012, **134,** 12406-12409.

23 P. L. Liao, M. C. Toroker and E. A. Carter, *Nano Lett.,* 2011, **11,** 1775-1781.

24 N. J. Cherepy, D. B. Liston, J. A. Lovejoy, H. M. Deng and J. Z. Zhang, *J. Phys. Chem. B,* 1998, **102,** 770-776.

25 J. H. Kennedy and K. W. Frese, *J. Electrochem. Soc.,* 1978, **125,** 709-714.

26 Cesar, A. Kay, J. A. G. Martinez and M. Gratzel, *J. Am. Chem. Soc.,* 2006, **128,** 4582-4583.

27 A. Glasscock, P. R. F. Barnes, I. C. Plumb and N. Savvides, *J. Phys. Chem. C,* 2007, **111,** 16477-16488.

28 A. Kay, I. Cesar and M. Graetzel, *J. Am. Chem. Soc.,* 2006, **128,** 15714-15721.

29 K. Sivula, R. Zboril, F. Le Formal, R. Robert, A. Weidenkaff, J. Tucek, J. Frydrych and M. Graetzel, *J. Am. Chem. Soc.,* 2010, **132,** 7436-7444.

30 J. Brillet, M. Gratzel and K. Sivula, *Nano Lett.,* 2010, **10,** 4155-4160.

31 L. Vayssieres, C. Sathe, S. M. Butorin, D. K. Shuh, J. Nordgren and J. H. Guo, *Adv. Mater.,* 2005, **17,** 2320-2323.

32 Y. Lin, S. Zhou, S. W. Sheehan and D. Wang, *J. Am. Chem. Soc.,* 2011, **133,** 2398-2401.

33 K. Q. Peng, Y. Wu, H. Fang, X. Y. Zhong, Y. Xu and J. Zhu, *Angew. Chem., Int. Ed.,* 2005, **44,** 2737-2742.

34 S. D. Tilley, M. Cornuz, K. Sivula and M. Graetzel, *Angew. Chem. Int. Ed.,* 2010, **49,** 6405-6408.

35 T. Hisatomi, H. Dotan, M. Stefik, K. Sivula, A. Rothschild, M. Graetzel and N. Mathews, *Adv. Mater.,* 2012, **24,** 2699-2702.

36 Y. Ling, G. Wang, J. Reddy, C. Wang, J. Z. Zhang and Y. Li, *Angew. Chem. Int. Ed.,* 2012, **51,** 4074-4079.

37 E. R. Young, R. Costi, S. Paydavosi, D. G. Nocera and V. Bulovic, *Energ Environ. Sci.,* 2011, **4,** 2058-2061.

38 Y. J. Hwang, C. H. Wu, C. Hahn, H. E. Jeong and P. Yang, *Nano Lett.,* 2012, **12,** 1678-1682.

39 K. Sun, Y. Jing, C. Li, X. Zhang, R. Aguinaldo, A. Kargar, K. Madsen, K. Banu, Y. Zhou, Y. Bando, Z. Liu and D. Wang, *Nanoscale,* 2012, **4,** 1515-1521.

40 X. Y. Yang, A. Wolcott, G. M. Wang, A. Sobo, R. C. Fitzmorris, F. Qian, J. Z. Zhang and Y. Li, *Nano Lett.,* 2009, **9,** 2331-2336.

41 F. Cardon and W. P. Gomes, *J. Phys. D: Appl. Phys.,* 1978, **11,** L63-L67.

42 A Novikov, *Solid-State Electron.,* 2010, **54,** 8-13.

43 Y. Xu, M. A. A. Schoonen, *Am. Mineral.,* 2000, **85,** 543-556.

44 A. Hagfeldt and M. Gratzel, *Chem. Rev.,* 1995, **95,** 49-68.

45 W. J. Albery and P. N. Bartlett, *J. Electrochem. Soc.,* 1984, **131,** 315-325.

46 X. Tan, P. E. Laibinis, S. T. Nguyen, J. M. Kesselman, C. E. Stanton and N. S. Lewis, *Prog. Inorg. Chem.,* 1994, **41,** 21-144.